Wireless Personal Communications (2024) 135:1103–1116
https://doi.org/10.1007/s11277-024-11110-6

Spectrum Sensing Using Intelligent Reflecting Surfaces with Multi-antennas Energy Harvesting

Raed Alhamad[1]

Accepted: 11 March 2024 / Published online: 4 May 2024

Abstract
In this paper, we suggest the use of Intelligent Reflecting Surfaces (IRS) to improve the spectrum sensing process using the energy detector and the throughput of Cognitive Radio Networks (CRN). The Primary Source (*PS*) harvests energy using the received signals on n_r antennas from node *A*. The harvested energy is employed to transmit data to Primary Destination *PD*. The transmitted signal is reflected by IRS so that all reflections have a null phase at Secondary Source *SS* where spectrum sensing is performed. Spectrum sensing using IRS equipped with $N = 32$ reflectors offers 27 dB and 30 dB gain when compared to spectrum sensing without IRS for a number of antennas $n_r = 2$ and 3 (Alhamad and Boujemaa in Wirel Pers Commun, 2021). We also suggest the use of IRS to increase the harvested energy and improve the spectrum sensing process. We also derive the primary throughput of CRN where the *PS* harvests energy using received signals on multiple antennas and there is an IRS that reflects *PS* signals to the *PD*. We derive the secondary throughput when the *SS* harvests energy and an IRS is located between the *SS* and the Secondary Destination *SD*.

Keywords IRS · 6G · Cognitive radio networks · Throughput analysis · Spectrum sensing · Energy harvesting

1 Introduction

IRS allow to enhance the throughput of wireless networks since all reflections have the same phase at the receiver [1–5]. IRS consists to adjust the phase shift of each reflector so that all reflected signals have a null phase at the receiver [6–8]. IRS can be employed as a reflector or a transmitter and allow significant performance enhancement of the order of 15, 21, 27 dB gain when compared to wireless systems without IRS for $N = 8, 16, 32$ reflectors. IRS have been proposed for Non Orthogonal Multiple Access [9], millimeter wave communications [10, 11] and optical communications [12]. IRS have been studied with continuous and discrete phase shifts [13–19]. IRS were not yet used to enhance spectrum

✉ Raed Alhamad
ralhamad@seu.edu.sa

[1] Information Technology Department, Saudi Electronic University, Riyadh, Kingdom of Saudi Arabia

sensing or the energy harvesting process as considered in this paper [20]. IRS was used in [21] to transmit packets to multiple users. Simultaneously Transmit and Reflect (STAR) IRS was suggested in [22] to broadcast data to users located in the transmit and reflect space of STAR-IRS. IRS using rate splitting was proposed in [23]. A survey on physical layer security using IRS was provided in [24]. IRS using beamforming was considered in [25]. IRS for millimeter wave communications was studied in [26]. Some experimental results have been performed to confirm the significant performance enhancement of wireless communication using IRS.

IRS have not been yet used to enhance the spectrum sensing process [20]. In fact, when the reflected signals have the same phase at the Secondary Source (*SS*), spectrum sensing will be performed with multiple signals with the same phase leading to an enhancement of detection probability. We consider that *PS* harvests energy using the received signals on n_r antennas from node *A*. The harvested energy is used to transmit data to *PD*. IRS is located between *PS* and *SS* so that all reflections have the same phase at *SS*. We show that the use of $N = 8, 16$ reflectors and $n_r = 2$ antennas offers 15 and 21 dB gain when compared to spectrum sensing without IRS [20]. Spectrum sensing using IRS equipped with $N = 32$ reflectors offers 27 dB and 30 gain when compared to spectrum sensing without IRS for a number of antennas $n_r = 2$ and 3 [20]. We also suggest the use of a second IRS to increase the harvested energy. IRS is located between node *A* and *PS* to increase the harvested energy since it uses multiple received reflected signals. The use of two IRS with $N_1 = N_2 = 8$ reflectors offers 30 dB and 8 dB gain when compared to spectrum sensing without IRS and a single IRS.

We also derive the primary and secondary throughput when IRS is located between Primary Source *PS* and Primary Destination *PD* and between Secondary Source *SS* and Secondary Destination *SD*. The use of a single IRS with $N = 8, 16, 32$ reflectors improves the throughput by 16, 22, 28 dB gain when compared to the absence of IRS. When two IRS with 8 reflectors are used, there is 35 dB gain when compared to the absence of IRS.

We consider the use of a single IRS located between the primary and the secondary source to enhance the spectrum sensing process. In fact, spectrum sensing uses the reflected signals on IRS that have the same phase. To enhance the energy harvesting process, we added a second IRS between node A transmitting RF signals and the primary source. The primary source uses the reflected signals on the second IRS during the energy harvesting process.

Sections 2 derives the detection probability when IRS is employed as a reflector. Section 3 evaluates the detection probability when IRS is employed as a transmitter. Section 3 suggests the use of a second IRS to increase the harvested energy. Numerical results are given in Sect. 4 while conclusions are presented in last section.

2 IRS Used as a Reflector

Figure 1 depicts the system model with a Primary Source (*PS*) equipped with n_r receive antennas used to harvest energy using the received signal from node *A*. The harvested energy is employed to transmit data to Secondary Destination *SD*. The transmitter signal is reflected on IRS equipped with *N* reflectors so that all reflections have the same phase

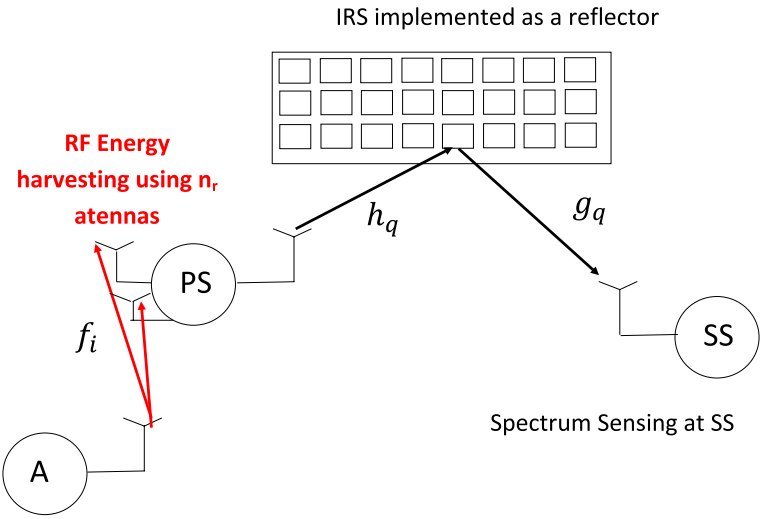

Fig. 1 Spectrum sensing using IRS as a reflector

at Secondary Source *SS* where spectrum sensing is performed using the energy detector. IRS is placed between the Primary source *PS* and the secondary source *SS*. IRS reflected the signals of *PS* so that they have the same phase at *SS*. A Rayleigh fading channel is used during the simulations.

The harvested energy at *PS* is expressed as

$$E = \mu\alpha T P_A \sum_{l=1}^{n_r} |f_l|^2 = \mu\alpha L_0 E_A \sum_{l=1}^{n_r} |f_l|^2, \tag{1}$$

where T_s is the symbol period, μ is the efficiency of energy conversion, $P_A = \frac{E_A}{T_s}$ is the power of node A, $L_0 = \frac{T}{T_s}$. The average power of channel coefficient f_l between A and l-th antenna of *PS* is $E(|f_l|^2) = \frac{1}{D_1^{ple}}$ where $E(X)$ is the expectation of X, D_1 is the distance between A and *PS* and *ple* is the path loss exponent.

The transmitted energy per symbol of *PS* is equal to E divided by the number of transmitted symbols ($L_0(1-\alpha)$):

$$E_{PS} = \frac{E}{L_0(1-\alpha)} = \frac{\mu\alpha E_A}{1-\alpha} \sum_{l=1}^{n_r} |f_l|^2. \tag{2}$$

Let h_q be the channel coefficient between *PS* and q-th reflector of IRS. Let g_q be the channel coefficient between q-th reflector of IRS and *SS*. h_q is a zero mean Gaussian random variable (r.v.) such that $E(|h_q|^2) = \frac{1}{D_2^{ple}}$ where D_2 is the distance between *PS* and IRS. g_q is a

zero mean Gaussian r.v. such that $E(|g_q|^2) = \frac{1}{D_3^{ple}}$ where D_3 is the distance between IRS and *SS*.

We have $h_q = a_q e^{-jb_q}$ where $a_q = |h_q|$ and b_q is the phase of h_q such that $E(a_q) = \frac{\sqrt{\pi}}{2\sqrt{D_2^{ple}}}$ and $E(a_q^2) = E(|h_q|^2) = \frac{1}{D_2^{ple}}$ [30]. We have $g_q = c_q e^{-jd_q}$ such that $E(c_q) = \frac{\sqrt{\pi}}{2\sqrt{D_3^{ple}}}$ and $E(c_q^2) = E(|g_q|^2) = \frac{1}{D_3^{ple}}$.

The phase of q-th reflector is [1]

$$\phi_q = b_q + d_q. \tag{3}$$

The received signal *SS* is written as

$$r_p = s_p \sqrt{E_{PS}} \sum_{q=1}^{N} h_q g_q e^{j\phi_q} + n_p. \tag{4}$$

where s_p is the p-th transmitted symbol, n_p is a Gaussian noise of variance N_0.

Using (3), we obtain

$$r_p = s_p \sqrt{E_{PS}} \sum_{q=1}^{N} a_q c_q + n_p. \tag{5}$$

The Signal to Noise Ratio (SNR) at *SS* is written as [1]

$$\gamma^{SS} = \frac{E_{PS}}{N_0} [\sum_{q=1}^{N} a_q c_q]^2, \tag{6}$$

Using (2), we obtain

$$\gamma^{SS} = \frac{\mu \alpha E_A}{(1-\alpha) N_0} \sum_{l=1}^{n_r} |f_l|^2 [\sum_{q=1}^{N} a_q c_q]^2, \tag{7}$$

For a large number of reflectors (i.e. $N \geq 8$) and using the Central Limit Theorem (CLT), $\sum_{q=1}^{N} a_q c_q$ follows a Gaussian distribution with mean $m = \frac{N\pi}{4\sqrt{D_2^{ple} D_3^{ple}}}$ and variance $\sigma^2 = \frac{N}{D_2^{ple} D_3^{ple}} [1 - \frac{\pi^2}{16}]$. As $[\sum_{q=1}^{N} a_q c_q]^2$ is non central chi-square r.v. and $\sum_{l=1}^{n_r} |f_l|^2$ is a central chi-square r.v. Therefore, γ^{SS} is the product of a non central chi-square r.v. and a central chi-square r.v. The Probability Density Function (PDF) of γ^{SS} is written as [27]

$$p_{\gamma^{SS}}(x) = \frac{N_0 (1-\alpha) e^{-0.5(\frac{m}{\sigma})^2} D_1^{ple}}{\mu \alpha E_A \Gamma(n_r)} \sum_{q=0}^{+\infty} \frac{(\frac{m}{\sigma})^{2q} 2^{\frac{-3q-n_r+1.5}{2}}}{q! \Gamma(q+0.5)}$$

$$\times K_{q-n_r+0.5}\left(\sqrt{\frac{2xD_1^{ple}N_0(1-\alpha)}{\alpha\mu E_A}}\right)\left(\frac{xD_1^{ple}N_0(1-\alpha)}{\mu\alpha E_A}\right)^{\frac{q+n_r-1.5}{2}} \tag{8}$$

We use [28]

$$\int_0^y \frac{2(CD)^{0.5C+0.5D}}{\Gamma(C)\Gamma(D)} x^{0.5C+0.5D-1} K_{C-D}(2\sqrt{CDx})dx$$

$$= \frac{1}{\Gamma(C)\Gamma(D)} G_{1,3}^{2,1}\left(CDy\middle| \begin{matrix} 1 \\ C,\ D,\ 0 \end{matrix}\right) \tag{9}$$

to obtain

$$\int_0^{\sqrt{x}} w^{A-1} K_B(w)dw = 2^{A-2} G_{1,3}^{2,1}\left(\frac{x}{4}\middle| \begin{matrix} 1 \\ \frac{A+B}{2},\ \frac{A-B}{2},\ 0 \end{matrix}\right) \tag{10}$$

where $G_{n,m}^{p,l}(x)$ is the Meijer G-function.

We deduce the Cumulative Distribution Function (CDF) of γ^{SS}:

$$P_{\gamma^{SS}}(x) = \frac{e^{-(\frac{m}{\sqrt{2}\sigma})^2}}{\Gamma(n_r)} \sum_{p=0}^{+\infty} \frac{(\frac{m}{\sigma})^{2p} 2^{-p}}{p!\Gamma(p+0.5)}$$

$$\times G_{1,3}^{2,1}\left(\frac{N_0(1-\alpha)xD_1^{ple}}{2\mu\alpha E_A}\middle| \begin{matrix} 1 \\ p+0.5,\ n_r,\ 0 \end{matrix}\right) \tag{11}$$

The detection probability at *SS* can be approximated by [20]

$$P_d \geq 1 - F_{\gamma^{SS}}(T^0), \tag{12}$$

where

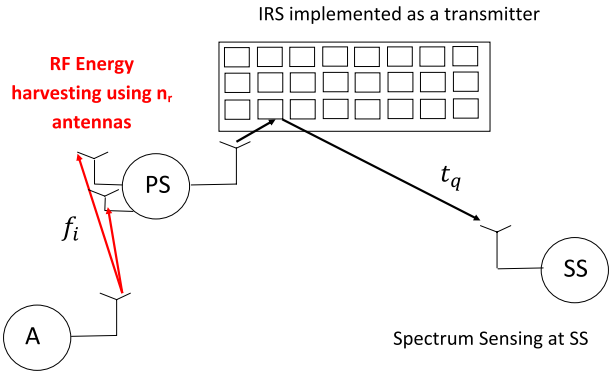

Fig. 2 Spectrum sensing using IRS is a transmitter

$$T^0 = \int_0^{+\infty} P_{nd}(x)dx \tag{13}$$

$P_{nd}(x) = 1 - Q_K(\sqrt{2Kx}, \sqrt{T})$ is the non detection probability of the energy detector using K samples and threshold T. $Q_K(x)$ is the Marcum Q-function.

3 Spectrum Sensing Using IRS Used as Transmitter

Figure 2 shows that spectrum sensing can be performed when IRS is employed as a transmitter. IRS is placed at *PS*. IRS is illuminated using the antenna of primary source *PS* [1]. Let ψ_q be the phase of the channel coefficient t_q between the q-th reflecting element of IRS and *SS*. We have $t_q = \rho_q e^{-j\psi_q}$ where $E(|t_q|^2) = \frac{1}{D_4^{ple}}$ and D_4 is the distance between *PS* and *SS*. From [30], we have $E(\rho_q) = \frac{\sqrt{\pi}}{2\sqrt{D_4^{ple}}}$ and $E(\rho_q^2) = \frac{1}{D_4^{ple}}$.

When IRS is deployed as a transmitter, the phase of q-th reflector is written as [1]

$$\Phi_q = \psi_q + e_m, \tag{14}$$

where $e_m = \frac{2\pi(m-1)}{M}$, $m = 1, \ldots, M$ is the phase of transmitted M-Phase Shift Keying symbol.

The received signal at *SS* is expressed as [1]

$$r_p = \sqrt{E_{PS}} \sum_{q=1}^{N} t_q e^{j\Phi_q} + n_p = \sqrt{E_{PS}} e^{je_q} \sum_{q=1}^{N} \rho_q + n_p. \tag{15}$$

The SNR at *SS* is equal to [1]

$$\gamma_2^{SS} = \frac{\mu\alpha E_A}{(1-\alpha)N_0} [\sum_{q=1}^{N} \rho_q]^2 \sum_{l=1}^{n_r} |f_l|^2, \tag{16}$$

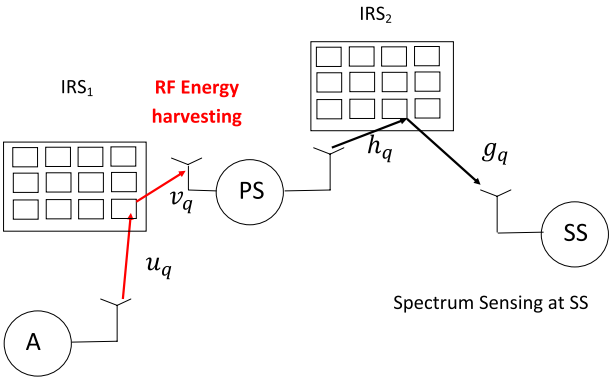

Fig. 3 Spectrum sensing using two IRS

For a large number of reflectors ($N \geq 8$) and using the Central Limit Theorem (CLT), $\sum_{q=1}^{N} \rho_q$ follows a Gaussian distribution with mean $m_2 = N\frac{\sqrt{\pi}}{2\sqrt{D_4^{ple}}}$ and variance $\sigma_2^2 = \frac{N(4-\pi)}{4D_4^{ple}}$. The CDF of γ_2^{SS} is given in (11) by replacing $\frac{m^2}{\sigma^2}$ by $\frac{m_2^2}{\sigma_2^2}$. The detection probability is evaluated as (12).

4 Spectrum Sensing Using Two IRS

Figure 3 depicts a system model containing two IRS: IRS_1 is used for increase the harvested energy with N_1 reflectors. IRS_1 is located between A and PS. IRS_2 is located between PS and SS, it contains N_2 reflectors to improve the spectrum sensing process.

When IRS_1 is used to increase the harvested energy, the harvested energy is equal to

$$E = \mu\alpha L_0 E_A [\sum_{l=1}^{N_1} \delta_l \eta_l]^2, \tag{17}$$

where $\delta_l = |u_l|$, u_l is channel coefficient between A and l-th reflector of IRS_1 and $\eta_l = |v_l|$ where v_l is the channel coefficient between l-th reflector of IRS_1 and PS.

For large values of $N_1 \geq 8$, $[\sum_{l=1}^{N_1} \delta_l \eta_l]$ follows a Gaussian distribution with mean $m_3 = \frac{N_1\pi}{4\sqrt{D_5^{ple} D_6^{ple}}}$ and variance $\sigma_3^2 = \frac{N_1}{D_5^{ple} D_6^{ple}}$. D_5 is the distance between A and IRS_1 and D_6 is the distance between IRS_1 and PS.

We can write the transmitted energy per symbol of PS as E given in (17) divided by the number of transmitted symbols ($L_0(1-\alpha)$)

$$E_{PS} = \frac{E}{L_0(1-\alpha)} = \frac{\mu\alpha E_A [\sum_{l=1}^{N_1} \delta_l \eta_l]^2}{1-\alpha} \tag{18}$$

The SNR at SS is equal to

$$\gamma_3^{SS} = \frac{E_{PS}[\sum_{q=1}^{N_2} a_q c_q]^2}{N_0}$$

$$= \frac{\mu\alpha E_A}{N_0(1-\alpha)} [\sum_{l=1}^{N_1} \delta_l \eta_l]^2 [\sum_{q=1}^{N_2} a_q c_q]^2. \tag{19}$$

where a_q, c_q were defined in Sect. 2 and N_2 is the number of reflectors of IRS_2.

As $[\sum_{l=1}^{N_1} \delta_l \eta_l]^2$ and $[\sum_{q=1}^{N_2} a_q c_q]^2$ are two non central chi-square r.v., γ_3^{SS} is the product of two non central chi-square r.v. The PDF of γ_3^{SS} is written as [27]

$$f_{\gamma_3^{SS}}(z) = e^{-\frac{m_3^2}{2\sigma_3^2} - \frac{m_4^2}{2\sigma_4^2}} \sum_{n=0}^{+\infty} \sum_{p=0}^{+\infty} \frac{2^{-2n-2p} (\frac{m_3}{\sigma_3})^{2p} (\frac{m_4}{\sigma_4})^{2n}}{n! p! \Gamma(n+0.5)\Gamma(p+0.5)}$$

$$\times \frac{N_0(1-\alpha)}{\mu\alpha E_A} K_{p-n}\left(\sqrt{\frac{N_0(1-\alpha)z}{\mu\alpha E_A}}\right)\left(z\frac{N_0(1-\alpha)}{\mu\alpha E_A}\right)^{\frac{p+n-1}{2}} \tag{20}$$

Using (10), the CDF of γ_3^{SS} is expressed as

$$P_{\gamma_3^{SS}}(z) = e^{-\frac{m_3^2}{2\sigma_3^2}-\frac{m_4^2}{2\sigma_4^2}} \sum_{n=0}^{+\infty}\sum_{p=0}^{+\infty} \frac{2^{-n-p}\left(\frac{m_3}{2\sigma_3}\right)^{2p}\left(\frac{m_4}{2\sigma_4}\right)^{2n}}{n!p!\Gamma(n+0.5)\Gamma(p+0.5)}$$

$$\times G_{1,3}^{2,1}\left(\frac{N_0(1-\alpha)z}{\mu\alpha E_A 4}\middle| \begin{matrix} 1 \\ p+0.5,\ n+0.5,\ 0 \end{matrix}\right) \tag{21}$$

where $m_4 = \frac{N_2^2\pi}{4\sqrt{D_2^{ple}D_3^{ple}}}$, $\sigma_4^2 = \frac{N_2^2}{D_2^{ple}D_3^{ple}}[1-\frac{\pi^2}{16}]$.

The detection probability is computed using (12) and (21).

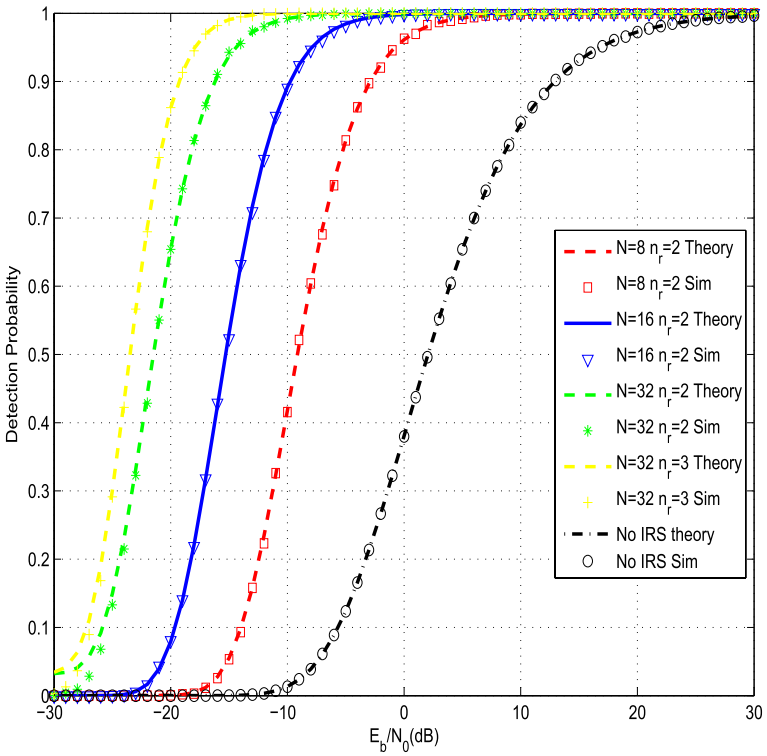

Fig. 4 Detection probability when IRS is deployed as a reflector

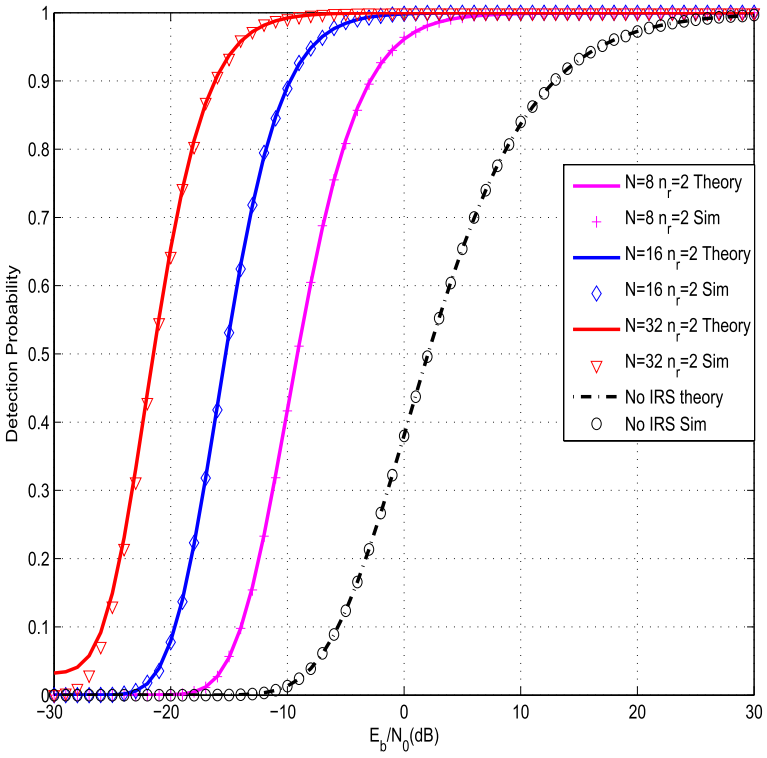

Fig. 5 Detection probability when IRS is deployed as a transmitter

5 Numerical Results

Figure 4 depicts the detection probability at *SS* using the energy detector over $K = 10$ samples with threshold $T = 1$ for $\mu = 0.5$. IRS is employed as a reflector, $ple = 3$ and the distances between nodes are $D_1 = 1.5$, $D_2 = 1.3$, $D_3 = 1.2$. When there are $N = 8, 16$ reflectors and $n_r = 2$, spectrum sensing using IRS offers 15 and 21 dB gain when compared to spectrum sensing without IRS [20]. When energy harvesting uses $n_r = 3$ antennas, spectrum sensing using IRS equipped with $N = 32$ reflectors offers 27 dB and 30 gain when compared to spectrum sensing without IRS for a number of antennas $n_r = 2$ and 3 [20]. In [20], spectrum sensing does not use IRS. Besides, IRS were not used to enhance the energy harvesting process in [20].

For the same parameters as Fig. 4, Fig. 5 depicts the detection probability with IRS employed as a transmitter. The distance between *PS* and *SS* is $D_4 = 2.5$. When there are $N = 8, 16, 32$ reflectors and $n_r = 2$, spectrum sensing using IRS offers 16, 22 and 28 dB gain when compared to spectrum sensing without IRS [20].

Figure 6 shows that the use of two IRS with $N_1 = N_2 = 8$ reflectors offers 30 dB and 8 dB gain when compared to spectrum sensing without IRS and a single IRS. The distance between A and IRS_1 is D_5 and the distance between IRS_1 and PS is $D_6 = 1.5$. The other parameters are the same as Fig. 4.

Figure 7 depicts the throughput at Primary Destination *PD* computed as

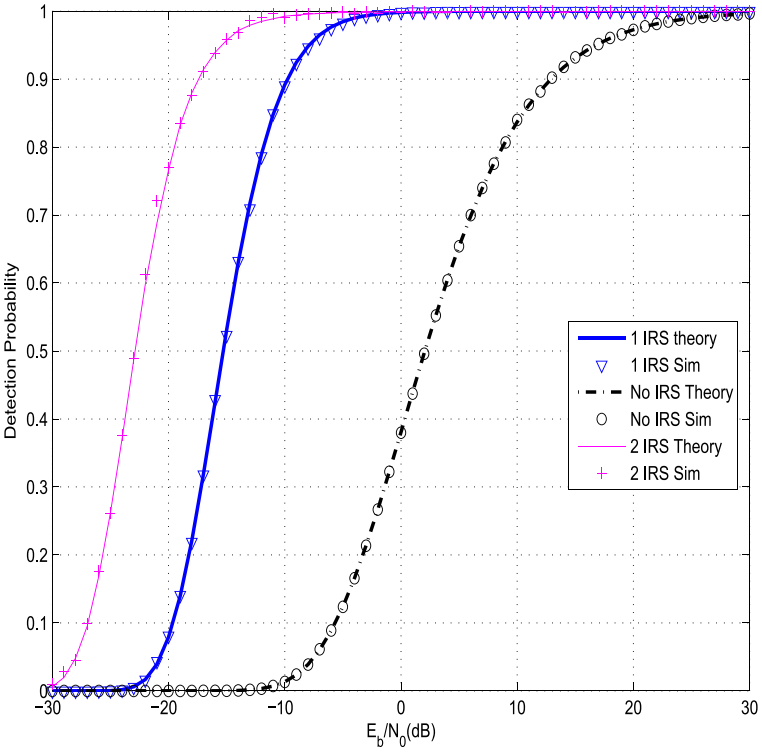

Fig. 6 Detection probability when IRS is used in energy harvesting and spectrum sensing: $N_1 = N_2 = 8$

$$Thr_{PD} = P_A(1-\alpha)[1 - PEP_{PD}]log_2(Q) \tag{22}$$

where Q is the size of the constellation size, P_A is the probability that PS is active, PEP_{PD} is the Packet Error Probability (PEP) at PD [29]

$$PEP_{PD} \leq F_{\gamma^{PD}}(W_0), \tag{23}$$

$F_{\gamma^{PD}}(x)$ is the CDF of SNR γ^{PD} at PD, expressed as (11) and (21) when there is a single IRS and two IRS, and W_0 is a waterfall threshold computed as [29]

$$W_0 = \int_0^{+\infty} [1 - SEP(w)]^{PL} dw \tag{24}$$

$SEP(w)$ is the Symbol Error Probability for (Q-QAM) [30]

$$SEP(w) = 2\left(1 - \frac{1}{\sqrt{Q}}\right) erfc\left(\sqrt{\frac{3w}{Q-1}}\right) \tag{25}$$

and $PL = 500$ is packet length.

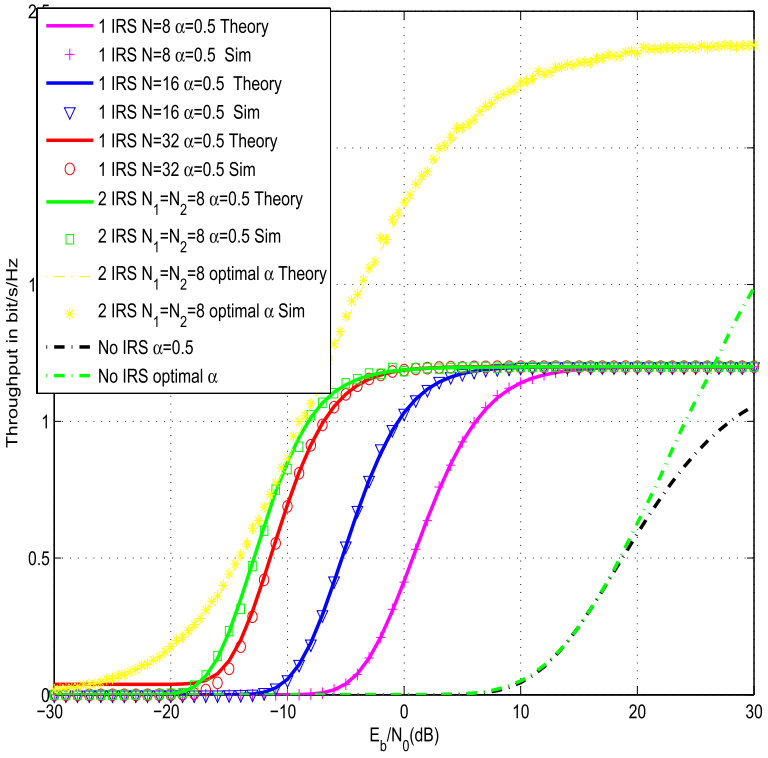

Fig. 7 Throughput in the primary network for 64QAM modulation: $P_a = 0.4$

Figure 7 shows that the use of $N = 8, 16, 32$ reflectors offers 16, 22 and 28 dB gain when compared to conventional systems without IRS. The probability that *PS* is active is $P_A = 0.4$. The use of two IRS with $N_1 = N_2 = 8$ reflectors offers 35 dB gain when compared to previous research results [20]. We also improved the throughput by optimizing the harvesting duration α.

Figure 8 depicts the secondary throughput at Secondary Destination (SD) for 64QAM modulation:

$$Thr_{SD} = [1 - P_A][1 - P_F](1 - \alpha)[1 - PEP_{SD}]log_2(Q) \tag{26}$$

where P_F is the false alarm probability, PEP_{SD} is the PEP at *SD* approximated by [29]

$$PEP_{SD} \leq F_{\gamma^{SD}}(W_0), \tag{27}$$

$F_{\gamma^{SD}}(x)$ is the CDF of SNR γ^{SD} at *SD* computed as (11) and (21). Figure 8 shows that the use of a single IRS with $N = 8, 16, 32$ reflectors offers 16, 22, 28 dB gain when compared to the absence of IRS. When we use 2 IRS with 8 reflectors, there is 35 dB gain when compared to the absence of IRS [20].

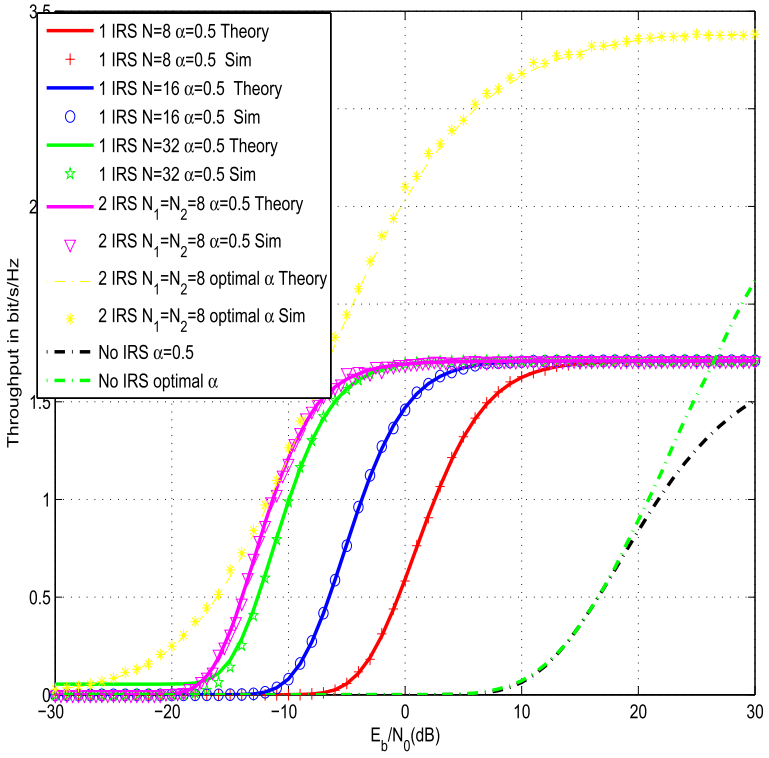

Fig. 8 Throughput in secondary network for 64QAM modulation: $P_a = 0.4$

6 Conclusions and Perspectives

In this paper, we suggested the use of Intelligent Reflecting Surfaces to improve the spectrum sensing process when the *PS* harvests energy on n_r receive antennas. IRS is located between *PS* and Secondary Source *SS* so that all reflections have a null phase at *SS* where the spectrum sensing process is performed. When there are $N = 8, 16$ reflectors and $n_r = 2$ antennas, spectrum sensing using IRS offers 15 and 21 dB gain when compared to spectrum sensing without IRS [20]. Spectrum sensing using IRS equipped with $N = 32$ reflectors offers 27 dB and 30 dB gain when compared to spectrum sensing without IRS for a number of antennas $n_r = 2$ and 3 [20]. We also suggested the use of IRS to increase the harvested energy and improve the spectrum sensing process. The use of two IRS with $N_1 = N_2 = 8$ reflectors offers 30 dB and 8 dB gain when compared to spectrum sensing without IRS and a single IRS. We also derived the primary and secondary throughput of CRN (Cognitive Radio Networks) with energy harvesting and using IRS. As a perspective, we can study other sources of energy such as solar or wind.

Author Contributions The paper is the contribution of Prof. Raed Alhamad.

Funding No Funding received for this paper.

Data Availability Data and material are not available.

Declarations

Conflict of interest The author states that there is no Conflict of interest for this paper.

References

1. Basar, E., Di Renzo, M., De Rosny, J., Debbah, M., Alouini, M.-S., & Zhang, R. (2019). Wireless communications through reconfigurable intelligent surfaces *IEEE Access*, *7*, 116753–116773.
2. Zhang, H., Di, B., Song, L., & Han, Z. (2020). Reconfigurable intelligent surfaces assisted communications with limited phase shifts: How many phase shifts are enough? *IEEE Transactions on Vehicular Technology, 69*(4), 4498–4502.
3. Di Renzo, M. (2019). 6G Wireless: Wireless networks empowered by reconfigurable intelligent surfaces. In *25th Asia-Pacific conference on communications (APCC)*.
4. Basar, E. (2020). Reconfigurable intelligent surface-based index modulation: A new beyond MIMO paradigm for 6G. *IEEE Transactions on Communications*, *68*(5), 3187–3196.
5. Wu, Q., & Zhang, R. (2020). Towards smart and reconfigurable environment: Intelligent reflecting surface aided wireless network. *IEEE Communications Magazine*, *58*(1), 106–112.
6. Huang, C., Zappone, A., Alexandropoulos, G. C., Debbah, M., & Yuen, C. (2019). Reconfigurable intelligent surfaces for energy efficiency in wireless communication. *IEEE Transactions on Wireless Communications*, *18*(8), 4157–4170.
7. Alexandropoulos, G. C., & Vlachos, E. (2020). A hardware architecture for reconfigurable intelligent surfaces with minimal active elements for explicit channel estimation. In *ICASSP 2020–2020 IEEE international conference on acoustics, speech and signal processing (ICASSP)*.
8. Guo, H., Liang, Y.-C., Chen, J., & Larsson, E. G. (2020). Weighted sum-rate maximization for reconfigurable intelligent surface aided wireless networks. *IEEE Transactions on Wireless Communications*, *19*(5), 3064–3076.
9. Thirumavalavan, V. C., & Jayaraman, T. S. (2020). BER analysis of reconfigurable intelligent surface assisted downlink power domain NOMA system. In *2020 International Conference on COMmunication Systems and NETworkS (COMSNETS)*.
10. Pradhan, C., Li, A., Song, L., Vucetic, B., & Li, Y. (2020). Hybrid precoding design for reconfigurable intelligent surface aided mmWave Communication Systems. *IEEE Wireless Communications Letters*, *9*(7), 1041–1045.
11. Ying, K., Gao, Z., Lyu, S., Wu, Y., Wang, H., & Alouini, M.-S. (2020). GMD-based hybrid beamforming for large reconfigurable intelligent surface assisted millimeter-wave massive MIMO. *IEEE Access*, *8*, 19530–19539.
12. Yang, L., Guo, W., & Ansari, I. S. (2020). Mixed Dual-Hop FSO-RF Communication Systems Through Reconfigurable Intelligent Surface. *IEEE Communications Letters*, *24*(7), 1558–1562.
13. Di, B., Zhang, H., Li, L., Song, L., Li, Y., & Han, Z. (2020). Practical hybrid beamforming with finite-resolution phase shifters for reconfigurable intelligent surface based multi-user communications. *IEEE Transactions on Vehicular Technology*, *69*(4), 4565–4570.
14. Nadeem, Q.-U.-A., Kammoun, A., Chaaban, A., Debbah, M., & Alouini, M.-S. (2020). Asymptotic max-min SINR analysis of reconfigurable intelligent surface assisted MISO systems. *IEEE Transactions on Wireless Communications*, *19*(12), 7748–7764.
15. Zhao, W., Wang, G., Atapattu, S., Tsiftsis, T. A., & Tellambura, C. (2020). Is backscatter link stronger than direct link in reconfigurable intelligent surface-assisted system? *IEEE Communications Letters*, *12*, 1256–1264.
16. Li, S., Duo, B., Yuan, X., Liang, Y.-C., & Di Renzo, M. (2020). Reconfigurable intelligent surface assisted UAV communication: Joint trajectory design and passive beamforming. *IEEE Wireless Communications Letters*, *9*(5), 716–720.
17. Hua, S., & Shi, Y. (2019). Reconfigurable intelligent surface for green edge inference in machine learning. In *2019 IEEE Globecom Workshops (GC Wkshps)*.
18. Huang, C., Alexandropoulos, G. C., Yuen, C., & Debbah, M. (2019). Indoor signal focusing with deep learning designed reconfigurable intelligent surfaces. In *2019 IEEE 20th international workshop on signal processing advances in wireless communications (SPAWC)*.

19. Dai, L., Wang, B., Wang, M., Yang, X., Tan, J., Bi, S., Xu, S., Yang, F., Chen, Z., Di Renzo, M., Chae, C.-B., & Hanzo, L. (2020). Reconfigurable intelligent surface-based wireless communications: Antenna design, prototyping, and experimental results. *IEEE Access*, *8*, 45913–45923.
20. Alhamad, R., & Boujemaa, H. (2021). Multihop multibranch spectrum sensing with energy harvesting. *Wireless Personal Communications* (to appear). *120*, 809–820
21. Verde, F., Darsena, D., & Galdi, V. (2024). Rapidly time-varying reconfigurable intelligent surfaces for downlink multiuser transmissions. *IEEE Transactions on Communications*(1), 1–1.
22. Naik, R. P. Salman, M., Bolboli, J., Savidhan, S. C. S., & Chung, W.-Y. (2024). Multiuser data transmission aided by simultaneous transmit and reflect reconfigurable intelligent surface in underwater wireless optical communications. *IEEE Transactions on Vehicular Technology*, Early Access, 1–14.
23. Li, H., Shen, S., & Clerckx, B. (2024). Synergizing beyond diagonal reconfigurable intelligent surface and rate-splitting multiple access. *IEEE Transactions on Wireless Communications*, (1), 1–1.
24. Kaur, R., Bansal, B., Majhi, S., Jain, S., Huang, C., & Yuen, C. (2024). A survey on reconfigurable intelligent surface for physical layer security of next-generation wireless communications. *IEEE Open Journal of Vehicular Technology, 5*, 172–199.
25. Gao, H., Yang, X., Chen, N., Chen, S., Yang, Y., & Yuen, C. (2024). Robust beamforming for reconfigurable intelligent surface-assisted multi-cell downlink transmissions. *IEEE Transactions on Vehicular Technology*, (1), 1–13.
26. Wang, R., Yang, Y., Makki, B., & Shamim, A. (2024). A wideband reconfigurable intelligent surface for 5g millimeter-wave applications. *IEEE Transactions on Antennas and Propagation*, *72*(3), 2399–2410.
27. Wells, W. T., Anderson, R. L., & Cell, J. W. (1962). The distribution of the product of two central or non-central chi-square variates. *The Annals of Mathematical Statistics, 33*(3), 1016–1020.
28. Najafi, M., Jamali, V., Diamantoulakis, P. D., Karagiannidis, G. K., & Schober, R. (2018). *Non-orthogonal multiple access for FSO backhauling*. IEEE WCNC.
29. Xi, Y., Burr, A., Wei, J. B., & Grace, D. (2011). A general upper bound to evaluate packet error rate over quasi-static fading channels. *IEEE Transactions on Wireless Communications, 10*(5), 1373–1377.
30. Proakis, J. (2007). *Digital communications* (5th ed.). Mac Graw-Hill.

Raed AlHamad received his B.S. at Information Systems Technology and Minor of Network Security from Southern Illinois University (SIUC), Carbondale, Illinois, in 2009, and the M.Eng. and Ph.D. degrees from Stevens Institute of Technology at Networked Information Systems in 2011 and Electrical Engineering in 2015, respectively. Also, In 2016 he got Edward Peskin Award. He has been with Saudi Electronic University since 2014. He is an associate professor, a head of Computer science and the vice dean of computing and informatics college. His research interests include wireless communications, networking, spectrum sensing and cyber security.